ELSEVIER

Chemical Engineering Science 60 (2005) 73–84

Chemical Engineering Science

www.elsevier.com/locate/ces

# Critical comparison of hydrodynamic models for gas–solid fluidized beds—Part II: freely bubbling gas–solid fluidized beds

D.J. Patil, M. van Sint Annaland*, J.A.M. Kuipers

*Department of Science and Technology, Twente University, P.O. Box 217, 7500 AE, Enschede, The Netherlands*

Received 12 December 2003; accepted 14 July 2004
Available online 11 September 2004

**Abstract**

Correct prediction of spontaneous bubble formation in freely bubbling gas–solid fluidized beds using Eulerian models, strongly depends on the description of the internal momentum transfer in the particulate phase. In this part, the comparison of the simple classical model, describing the solid phase pressure only as a function of a solid porosity by an empirical correlation and assuming the solid phase viscosity constant, which is referred to as the constant viscosity model (CVM), with the more fundamental model based on the kinetic theory of granular flow (KTGF), in which the solid phase properties are described in much more detail in terms of instantaneous binary particle–particle interactions, has been extended for freely bubbling fluidized beds. The performance of the KTGF and the CVM in predicting the hydrodynamics of freely bubbling fluidized beds has been compared with experimental data and correlations taken from the literature.

In freely bubbling fluidized beds at relatively low gas velocities, bubble formation is initiated by inelastic particle–particle interactions. When accounting for the dissipation of granular energy by particle collisions, the KTGF predicts much larger bubbles with a much sharper interface in comparison to the CVM. The average bubble size distribution predicted by the KTGF showed better agreement with correlations as well as experimental data from the literature. Although both models showed an increase in the predicted average bubble size with increasing superficial gas velocities, the discrepancy in the predicted bubble size becomes smaller, indicating the growing importance of the gas particle interactions in the bubble formation process at higher gas velocities. The rise velocity predicted by the KTGF and the CVM is approximately the same and in good agreement with correlations available in the literature. Since the KTGF predicts somewhat larger bubbles, also the predicted visible bubble flow is higher in comparison to the CVM.

In very dense regions in the fluidized bed the KTGF based on instantaneous binary collisions needs to be extended for additional frictional stresses in addition to the kinetic and collisional transport mechanisms. The extra frictional stresses were implemented via a relatively simple semi-empirical closure model and proved to have a significant influence on the predicted bubble size, rise velocity and visible bubble flow rate, where the model predictions strongly depend on the empirical constants. To further enhance the performance of the KTGF to describe the hydrodynamics of freely bubbling beds a more fundamental description of the frictional stresses on the particle level should be incorporated.


*Keywords:* Gas-solid fluidized beds; Bubble formation

## 1. Introduction

In freely bubbling fluidized beds consisting of Geldart B or D type particles (Geldart, 1973) with a superficial gas velocity exceeding the minimum fluidization velocity, spontaneous bubble formation starts at the distributor plate with tiny bubbles. When the bubbles rise through the fluidized bed, they grow due to entrained gas and coalescence with other bubbles. Many heat and mass transfer properties of the fluidized bed can be related directly to the presence of bubbles, and are dominated by their behavior. Therefore, a fundamental understanding of the hydrodynamics

* Corresponding author. Tel.: +31-53-489-4478; fax: +31-53-489-2882.
*E-mail address:* m.vansintannaland@utwente.nl
(M. van Sint Annaland).

0009-2509/$ - see front matter © 2004 Elsevier Ltd. All rights reserved.
doi:10.1016/j.ces.2004.07.058

including an accurate prediction of the bubble characteristics, such as the bubble size distribution is of great practical importance. For the description and ultimately the design of a fluidized bed reactor computational fluid dynamics (CFD) has become an emerging tool for better understanding and prediction of the complex flow structures. In the Eulerian approach to model gas–solid fluidized beds, closures are required for the internal momentum transfer in the particulate phase (solid phase viscosity and solid phase pressure gradient). Previously, the solid phase pressure was defined only as a function of the local solid porosity via empirical correlations and the solid phase viscosity was assumed constant. This model is referred as the constant viscosity model (CVM) (Gidaspow and Ettehadieh, 1983; Kuipers, 1990). In recent years, expressions for solid phase stress tensors have been developed by applying the dense gas kinetic theory to particle assemblies (Ding and Gidaspow, 1990). As a result of shearing of the particulate phase in a fluidized bed, particles collide with each other generating a random component in the particle motion. This particle velocity fluctuation generates an effective pressure in the particulate phase, together with an effective viscosity that resists the sharing of the particle assembly. Although this recent model, based on the kinetic theory of granular flow (KTGF), gives a more fundamental insight of the particle–particle interactions, a critical comparison of the performance of both models against available experimental data has not been carried out yet. In recent studies (for example Boemer et al., 1998; van Wachem, 2000) a frictional contribution to the momentum transfer in the solid phase, which is dominant in dense regions of the fluidized bed, has been accounted for using empirical correlations based on soil mechanics. However, the influence of these additional stresses on the bubble dynamics is not clear. In Part I the CVM and KTGF model were described and the performance of these models were compared in their prediction of the size of the start-up bubble and the time-averaged axial porosity profiles in a fluidized bed operated with a jet. This comparison will be extended in this part to freely bubbling fluidized beds.

Almost all the contributions in the literature on the simulation of gas–solid fluidized beds is limited to a qualitative comparison due to the high required computational costs of the simulations as well as lack of reliable experimental data to validate the calculations. Recently, van Wachem (2000) extracted quantitative information like bubble size distribution and bubble rise velocity from simulation results to validate his model. Following his approach, in this work the bubble size distribution, bubble rise velocity and visible bubble flow rate in a freely bubbling fluidized bed for Geldart B as well as D type particles predicted by the KTGF and the CVM were compared with generally accepted correlations as well as experimental data taken from the literature. Firstly, the CVM and KTGF models are analyzed for different constitutive equations available in the literature followed by a description of the classical approach for the estimation of the bubble size distribution in the bed and rise velocity as a function of the bubble diameter. Subsequently, the calculated averaged bubble size as a function of the height above the gas distributor and the bubble rise velocity as a function of the bubble diameter for 500 and 692 μm particle sizes are compared with available correlations from the literature and experimental data. Finally, the influence of the frictional stresses in the prediction of the bubble size and bubble rise velocity is studied.

## 2. Numerical simulations

The two-fluid model equations were implemented in the commercial CFD code CFX4.4 from AEA Technology, Harwell, UK. For the evaluation of the convective terms the third-order total variation diminishing (TVD) scheme min-mod was used. Simulations with the CVM and KTGF were carried out for a two-dimensional fluidized bed of size 0.57 m × 1.0 m with a particle size of 500 μm (Geldart B) and 692 μm (Geldart D). The experimental data of bubble size distribution, rise velocity and volumetric bubble flow reported by the Boemer et al. (1998) for the particle size of 692 μm were used for the comparison of the model predictions. The physical properties of the gas and the solid phase and the operating conditions have been listed in Table 1. In the experiments, to distribute gas with uniform velocity through the distributor porous plates are used (Hilligardt and Werther, 1986; Boemer et al., 1998). In reality gas velocity at the distributor plate cannot remain uniform along the cross-section due to non-uniform pressure drop across the porous plate. However, in the simulations uniform gas velocity inlet is assumed at the distributor plate. The simulations were carried out with a superficial gas velocity of 1.5, 2 and 2.5 times minimum fluidization velocity ($u_{mf}$) for a bed filled with Geldart B type particles and with $2u_{mf}$ for a bed filled with Geldart D type particles. A uniform grid of 0.01 m in the vertical direction and 0.0075 m in the horizontal direction was used. Preliminary calculations with a more refined grid (0.005 m × 0.005 m) showed that the time-averaged results were within 5% variation. Appendix A shows a comparison of the average bubble size calculated from the simulations with different grid size. Time steps of $3 \times 10^{-4}$ and $1 \times 10^{-4}$ s were used for CVM and KTGF model calculations, respectively.

## 3. Literature correlations

In freely bubbling fluidized bed small bubbles form at the bottom of the fluidized bed, which rise, coalesce, and erupt as large bubbles at the fluidized bed surface. Werther and Molerus (1973) developed a small capacitance probe and used a statistical theory to measure the bubble diameter and the bubble rise velocity in fluidized beds. The capacitance probe was placed in the fluidized bed at different

Table 1
Physical properties of the gas and solids and operating conditions

| | Geldart B | Geldart D |
|---|---|---|
| Particle diameter (μm) | 500 | 692 ( Boemer et al., 1998) |
| Particle density (kg/m$^3$) | 2660 | 2545 |
| Gas density (kg/m$^3$) | 1.2 | 1.2 |
| Gas viscosity (Pa s) | $1.85 \times 10^{-5}$ | $1.85 \times 10^{-5}$ |
| Restitution coefficient dimensionless | 1.0, 0.95 | 0.95 |
| $u_{mf}$ (m/s) | 0.222 | 0.338 |
| Freeboard pressure (N/m$^2$) | $1.013 \times 10^5$ | $1.013 \times 10^5$ |

Table 2
Different correlations presented in the literature for the estimation of the bubble size distribution

| Author | Correlation | Particle type | Bed Geometry | $D_0$ |
|---|---|---|---|---|
| Darton et al. (1977) | $D_b = 0.54(u-u_{mf})^{0.4}(h+4\sqrt{A_0})^{0.8}g^{-0.2}$ | | | |
| | $4\sqrt{A_0} = 0.03\ m$ (Porous plate) | B | 3D | — |
| Hilligardt and Werther (1986) | $D_b = D_0(1+27(u-u_{mf}))^{1/3}(1+6.4h)^{1.2}$ | A, B and D | 3D | (Solid A) 0.0061<br>(Solid B) 0.0085<br>(Solid D) 0.0123 |
| | | D | 2D | (Solid D) 0.01955 |
| Lim et al. (1993) | $D_b = \left[\frac{8(u-u_{mf})(2^{3/4}-1)}{\pi c g^{1/2}}h + D_0^{3/2}\right]^{2/3}$ | B and D | 2D | $D_0 = \left[\frac{8(u-u_{mf})A_0}{\pi\lambda g^{1/2}}\right]^{2/3}$<br>$A_0 = 5.6 \times 10^{-5}\ \mathrm{m}^2$<br>(Porous plate) |

heights and at different radial positions in the bed. The bubble rise velocity was determined using two vertically spaced probes. The capacitance probe measured the bubbles passing it, i.e. the bubbles that were pierced by the capacitance probe. The duration of this piercing depends on the size of the bubble, the bubble rise velocity, and the position of the bubble relative to the probe. From the measured distribution of the pierced length, the size distribution of the bubble was determined using a geometrical probability theory. Different correlations for the average bubble diameter proposed in the literature have been presented in Table 2, where $D_b$ is the bubble diameter, $h$ is the height of the bubble above the inlet of the fluidized bed, $u$ is the actual superficial gas inlet velocity, and $A_0$ is the 'catchment area', which characterizes the distributor. The basis of the model by Darton et al. (1977) is that bubbles tend to rise in preferred paths and that the distance traveled by two neighboring bubbles before coalescing is proportional to their lateral separation. Darton et al. (1977) validated their model with measurements carried out by Werther (1974) and many other researchers.

To model growth of circular bubbles in a two-dimensional fluidized bed, Lim et al. (1993) adopted an approach parallel to that developed by Darton et al. (1977) for spherical bubbles in three-dimensional beds. The proportionality constant $c$, used in the correlation by Lim et al. (1993) describes the distance the bubble travels in a stream before coalescing with an adjacent stream to form a single stream of large bubbles, and was found to be $\sim 2$.

The bubble rise velocity can be expressed by a generalized form of the Davidson and Harrison (1963) bubble model (Hilligardt and Werther, 1986):

$$u_b = \psi(U - U_{mf}) + \varphi v\sqrt{gD_b}, \tag{1}$$

The values of the empirical coefficients $\psi$, $\varphi$ and $n$, added by Hilligardt and Werther (1986), are empirical coefficients based on their data, which depend on the type of particles and the width and height of the fluidized bed and have been listed in Table 3. The parameter $\psi$ can be interpreted as the deviation of the visible bubble flow rate, $\dot{V}_b$, from the two-phase theory. However, it should be noted that the correlations given by Hilligardt and Werther (1986) for Group D type particles are based on the experiments performed with 480 μm particles, which are categorized as B type particles according to Geldart classification and type D from the classification done by Molerus (1982).

## 4. Results

### 4.1. Mechanism of spontaneous bubble formation

When the superficial gas velocity exceeds the minimum fluidization velocity, spontaneous bubble formation starts at the distributor plate, where tiny bubbles are formed. When the bubbles rise through the fluidized bed, they grow due to entrained gas and coalescence with other bubbles. Due

Table 3
Values for the empirical constants in the generalized equation for the bubble rise velocity (Eq. (1)), as proposed by different researchers

| | Bed Geometry | Particle sizes (μm) | $\psi$ | $\varphi$ | $v$ |
|---|---|---|---|---|---|
| Davidson and Harrison (1963) | 3D | — | 1.0 | 0.71 | 1.0 |
| Ocone et al. (1993). | 2D | 100–760 | — | 0.48 | 1.0 |
| Hilligardt and Werther (1986) | 3D | 480 | 0.26 for $h/D_t < 0.55$ | 0.71 | 0.87 |
| | | | $0.35(h/D_t)^{1/2}$ for $h/D_t < 0.55$ | | $0.05 \leqslant D_t \leqslant 1.0$ m |
| Lim et al. (1993) | 2D | 240–725 | 1 | 0.40 | 1.0 |

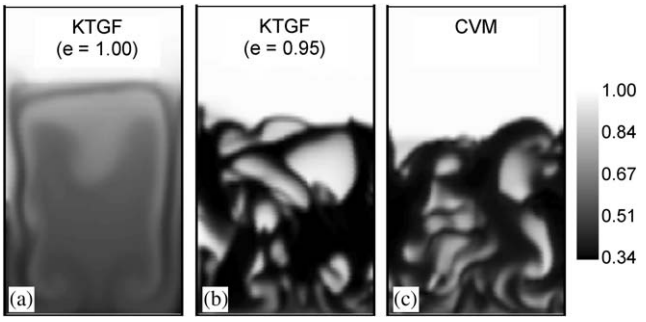


Fig. 1. Snapshots of the porosity profile predicted after 0.9 s for a freely bubbling fluidized bed filled with 500 μm particles and a superficial gas velocity of $2u_{mf}$, for: (a) KTGF assuming fully elastic collisions ($e = 1$), (b) KTGF assuming slightly inelastic collisions ($e = 0.95$), (c) CVM.

to the increasing bubble diameter the bubbles rise faster, thus increasing the level of the bed (Boemer et al., 1998). Fig. 1 shows snapshots of the porosity distribution calculated by the CVM and the KTGF with a particle–particle restitution coefficient of 1.0 and 0.98 for a two-dimensional bed filled with 500 μm particles with a superficial gas velocity of $2u_{mf}$. The porosity plot calculated by the KTGF assuming fully elastic particles shows a uniform bed expansion without any bubbles and the CVM predicts very small and diffuse bubbles (whose shape deviates from the typical experimentally observed spherical-cap shape). However, the KTGF, assuming slightly inelastic collisions, predicts much larger spherical cap shaped bubbles with a much sharper bubble interface, especially near the top of the bed. The prediction by the KTGF is consistent with the result of Euler–Lagrange simulation reported by Hoomans et al. (1996) and corresponds better with the experimental observations.

In the simulations of a freely bubbling bed, an initial pressure and corresponding voidage wave is propagated through the bed due to the start-up conditions. In the KTGF model accounting for inelastic collisions, granular energy is dissipated and the granular temperature is in the order of magnitude of $10^{-5}\,\mathrm{m^2/s^2}$, which is much lower than the level of the granular temperature in the KTGF assuming fully elastic particle–particle collisions ($10^{-3}\,\mathrm{m^2/s^2}$). Due to the dissipation of the fluctuating energy, the particles remain much closer together, resulting in a local compaction of the solid phase, which increases the drag experienced by the gas phase resulting in the formation of a bubble. In the KTGF assuming fully elastic collisions, the compaction of the particles is insufficient due to the relatively high granular energy, which results in a uniform bed expansion without any bubbles. Additional calculations with the CVM showed that decreasing the solid phase viscosity indeed increases the bubble size but still very diffuse bubbles are predicted. The CVM can be considered as a simplified KTGF model, where a uniform and constant granular energy in the entire fluidized bed is assumed and the local variation and therefore the influence of convection, diffusion, generation and dissipation of granular energy on the momentum transport properties of the particulate phase is entirely ignored. From the tiny bubbles observed in the calculation by the CVM, it can be concluded that the implicitly assumed granular energy level (via the assumed solid phase viscosity and elasticity modulus) was lower than in the calculation with the KTGF model with fully elastic collisions, but still higher than in KTGF calculation with $e = 0.95$. Since for all viscosities the CVM model predicts diffuse bubbles, not only the level of granular energy in the bed is important, but also the local distribution of the granular temperature. Due to the non-linear drag dependency on the solid volume fraction the tiny bubbles act as seeds for bubble formation in the CVM, which grow in time. Although bubble formation was predicted by the CVM, the average bubble size predicted by the CVM was much smaller than the KTGF model assuming inelastic collisions.

### 4.2. Quantitative comparison of the model results

In order to compare the predicted bubble sizes predicted by the KTGF and CVM quantitatively with experimental data, the equivalent bubble diameter of every individual bubble was calculated. Although there is no general agreement on the definition of a bubble diameter, for the current analysis of the simulation results, the equivalent bubble diameter was defined as the diameter of a circle with the same area as the numerically computed area for which $\varepsilon_f > 0.85$. Many correlations have been published in the literature (see Table 2) to describe the average bubble size as a function of the bed height. A comparison of the model results with these empirical correlations for the average bubble size requires the calculation of the mean bubble diameter. The determination of the mean bubble diameter requires careful consideration, since it is not always exactly clear what authors have actually measured in reality. Have they taken all the bubbles into

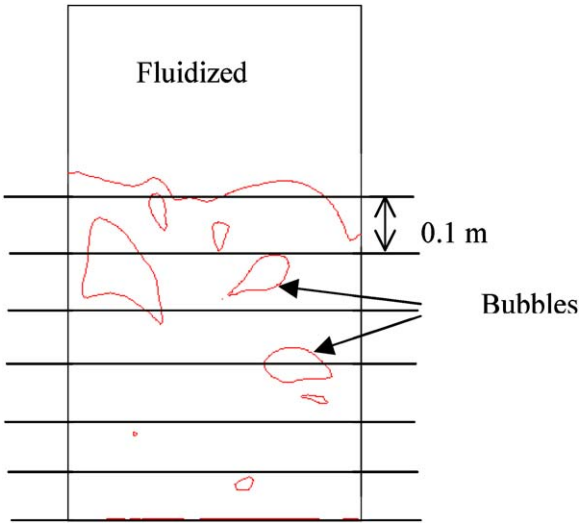


Fig. 2. Approach for the calculation of the average bubble diameter at different heights above the distributor in the fluidized bed.

account, or only the larger bubbles? Have they included effects such as coalescence, break-up, and wall effects? When comparing model results to measurements, it is important to retrieve similar data from the model and the measurements.

The fluidized bed was divided into different sections of uniform height (0.1 m) as indicated in Fig. 2. A location of the bubble was determined by calculating the center of mass of the bubble and assuming it as a point property. The diameters and centers of all bubbles in the bed for all sections of the fluidized bed were recorded at regular time interval (0.001 s). All simulations were carried out for 9 s of real time. To avoid the start-up effect, the average bubble diameter was calculated by averaging over the period of 1–9 s. Additional calculations showed that increasing the averaging time did not change the time-averaged results (see Appendix B). Fig. 3 shows the histogram of the percentage of the total number of bubbles (number distribution) and area distribution over the different bubble size groups for a lower section (from 0.1 to 0.2 m above the distributor) and a higher section (from 0.4 to 0.5 m above the distributor) of the fluidized bed predicted by the KTGF model for a superficial gas velocity of $2u_{mf}$. Fig. 3 shows that the relatively small bubbles at the lower section grow into much larger bubbles with a very broad distribution at somewhat higher positions in the bed. Although the smaller bubbles are still larger in numbers at the upper section, the larger bubbles contribute relatively more to the total bubble hold-up. Detailed inspection of the calculation results revealed that the smaller bubbles at the higher section of the fluidized bed were created during bubble–bubble interactions (coalescence and break-up). It should be noted that since the size and position of all the bubbles in all sections of the fluidized bed were recorded at regular time intervals, there is a possibility that smaller bubbles were counted more frequently than the larger bubbles due to the lower rise velocity of the smaller bubbles. In

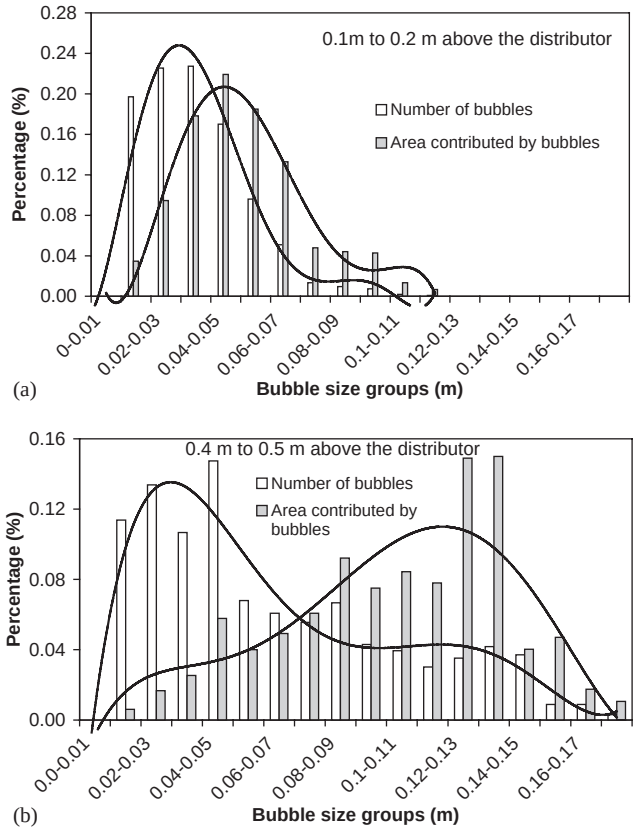


Fig. 3. Local distribution of the number of bubbles and area contributed by bubbles for different bubble size groups in (a) a lower section (from 0.1 to 0.2 m above the distributor) and (b) a higher section (from 0.4 to 0.5 m above the distributor) of the fluidized bed ($d_p = 500\,\mu m$, $u = 2u_{mf}$), calculated with the KTGF model. The line represents the trend of the variation.

the experimental determination of the average bubble size, a probe measurement is carried out in which every bubble is counted only once. However, mimicking this experimental procedure in the simulations would require extremely large computational times due to the very large real time to be simulated.

### 4.2.1. Average bubble diameter

Due to the difference in the number distribution and contributed area distribution, the definition of the average bubble diameter in each section of fluidized bed is not straightforward. If $N$ is the number of bubbles in one section and if $D_i$ is the diameter of bubble $i$ estimated from its area $A_i$, then a simple number averaging gives,

$$D_b = \frac{\sum D_i}{N}. \tag{2}$$

However, for the transport processes relevant average bubble volume cannot be obtained from the cube of the mean volume of the number density distribution (Werther, 1974). In the development of the bubble growth model, Darton et al. (1977) assumed that coalescence of bubbles in a

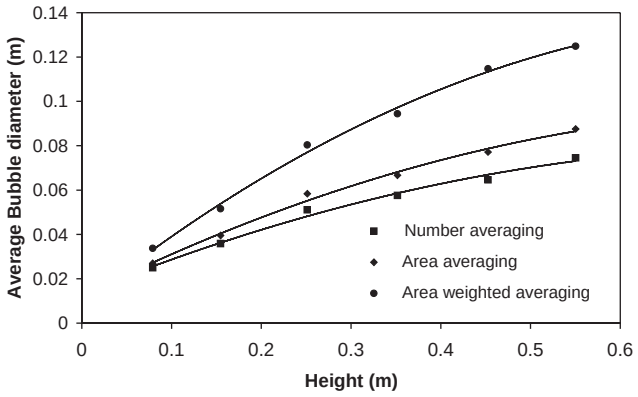


Fig. 4. Comparison of the average bubble diameter predicted by different averaging methods as a function of bed height ($d_p = 500\,\mu m$, $u = 2u_{mf}$) predicted by the KTGF model.

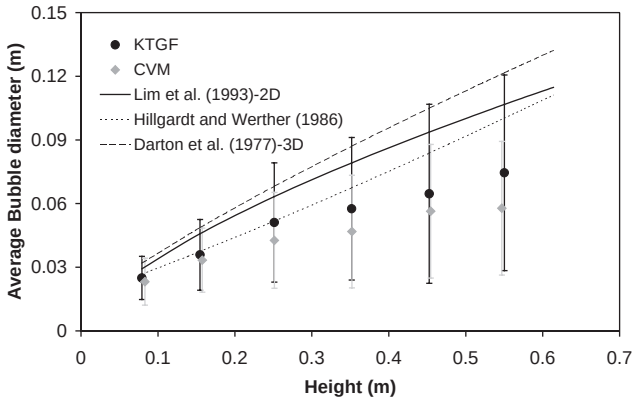


Fig. 5. Comparison of the number-averaged bubble diameter as a function of height above the distributor predicted by the KTGF and the CVM with different correlations in the literature ($d_p = 500\,\mu m$, $u = 2u_{mf}$).

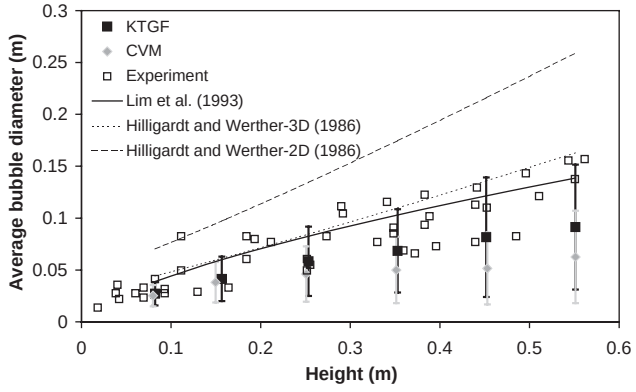


Fig. 6. Comparison of the number-averaged bubble diameter as a function of height above the distributor predicted by KTGF and CVM with different correlations in the literature ($d_p = 692\,\mu m$, $u = 2u_{mf}$).

fluidized bed leads to growth of the bubble size with increasing distances above the distributor. In other words, all the bubbles in the lower section of the fluidized bed coalesce when rising to the upper section and grow. As a result, the total bubble volume remains the same. In this case, the average bubble size represents the average bubble volume and can be estimated as the diameter of a sphere having the same volume as the average volume of the bubble. In a two-dimensional fluidized bed the average bubble size represents the average area of the bubble and can be estimated as the diameter of a circle having the same area as the average bubble area. This can be termed as area averaging:

$$A_b = \frac{\sum A_i}{N} \quad \text{and} \quad D_b = \sqrt{\frac{4A_b}{\pi}}. \tag{3}$$

Although the frequency of small bubbles and large bubbles is in the same order of magnitude, the larger bubbles will dominate the transport properties inside a fluidized bed. Therefore, in order to take into account the center of gravity of the distribution, the area weighted mean bubble diameter was calculated given by

$$D_b = \frac{\sum A_i D_i}{\sum A_i}. \tag{4}$$

The bubble size as a function of height in the fluidized bed calculated by the KTGF using different averaging techniques is presented in Fig. 4. The graph shows that the predicted bubble size increases with increasing distances from the distributor. The average bubble size calculated by the area weighted averaging method was much larger than by the area averaging method or the number averaging method.

A comparison of the number-averaged bubble size calculated by the KTGF and CVM and literature correlations is given by Fig. 5, showing that the average bubble size predicted in the KTGF is somewhat larger than predicted by the CVM. The difference in the prediction of the average bubble size by the KTGF and the CVM increases as the distance above the distributor increases. Additionally, The average bubble size predicted by the KTGF and the CVM, especially in the higher section of the fluidized bed, was lower than that estimated by any of these correlations. However, the bubbles size predicted by the models showed a very large distribution, which is indicated in the figure with the error bars. The error bars in the figure indicate the deviation of this bubble diameter, computed from the root mean square (RMS) of the deviation of bubble diameter from average bubble diameter:

$$\mathrm{RMS}\langle D_b \rangle = \sqrt{\frac{\sum (D_b - D_i)^2}{N}}. \tag{5}$$

Fig. 6 illustrates a comparison of the average bubble size predicted by the KTGF and the CVM with experimental data reported by Boemer et al. (1998). Although the experimental data is based on digital image analysis, the bubble diameter was not averaged. The graph shows that the average bubble size predicted by the KTGF was in reasonably close agreement with the experimental measurements. The average bubble size predicted by both models was also compared with different well-known correlations published in

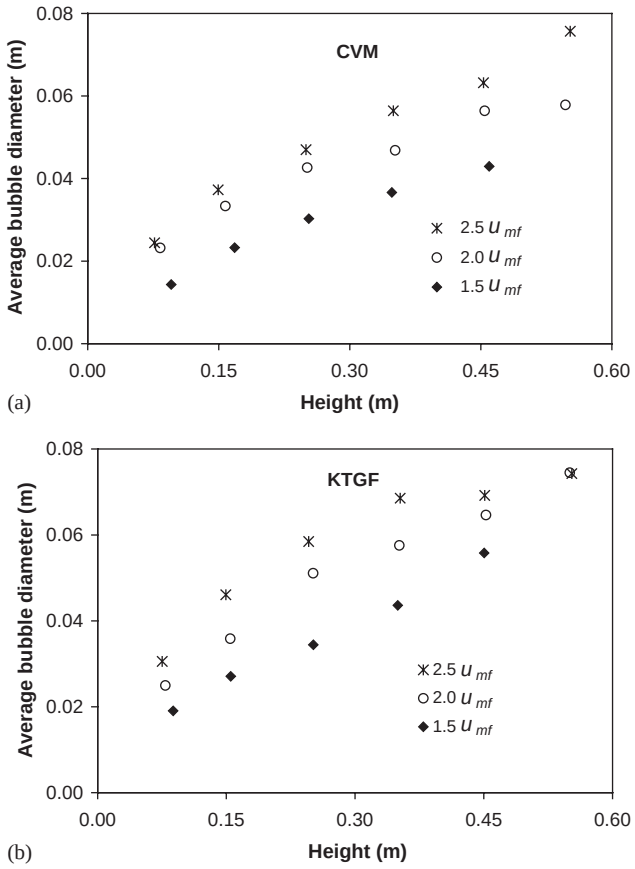


Fig. 7. (a and b) Number-averaged bubble size predicted by (a) CVM and (b) KTGF model for different superficial gas velocities (1.5, 2.0 and 2.5 times $u_{mf}$) for the fluidized bed filled with 500 μm particles.

the literature. The bubble size estimated with a correlation by Darton et al. (1977) for 3D fluidized bed is slightly larger than calculated by the correlation presented by Hilligardt and Werther (1986). The bubble size determined by the correlation given by Lim et al. (1993) for 2D fluidized bed is somewhat lower than estimated by the correlation by Darton et al. (1977) but somewhat higher than that predicted by Hilligardt. This suggests that the bubble size varies significantly depending upon particle size and bed geometry. As noted before, the correlations were based on probe measurements in which every bubble was counted only once irrespective of its size. In contrast, in our simulations due to lower rise velocity smaller bubbles were counted more frequently, which lowered the average bubble diameter.

#### 4.2.2. Influence of the gas velocity

The influence of the superficial gas velocity on the number-averaged bubble diameter predicted by the CVM and the KTGF as a function of height above the distributor is plotted in Fig. 7. The average size of the bubbles increases with an increase in the superficial gas velocity. The values for the number-averaged bubble size predicted by the KTGF are somewhat higher than those predicted by the CVM for all the gas velocities, however the difference between the predicted average bubble diameters decreases at higher gas velocities. This can be explained by a shift in the dominant mechanism of the bubble formation from inelastic particle–particle collisions at low gas velocities to the non-linear drag experienced by particulate phase at higher gas velocities. The influence of the height and gas velocity was also studied by fitting the exponent A and B in the generalized Darton's equation:

$$D_b = \text{constant}(u - u_{mf})^A (h + 4\sqrt{A_0})^B g^{-0.2}. \quad (6)$$

The exponent $A$ was estimated from the slope of the graph plotting $\log_{10}(h+4\sqrt{A_0})$ vs. $\log_{10}(D_b)$ for different superficial velocities and exponent $B$ was estimated from the slope of the graph showing $\log_{10}(u - u_{mf})$vs. $\log_{10}(D_b)$for different heights. The results have been summarized in Table 4. The average value of $A$ and $B$ predicted by both models is in close agreement with the exponent proposed by Darton et al. (1977), 0.4 and 0.8, respectively. The values found for exponent $A$ predicted by both models showed that at lower heights the bubble size is a stronger function of the superficial gas velocity and this dependency decreases slightly with increasing heights. Similarly, the value found for exponent $B$ showed that the influence of the height above the distributor is higher for lower gas velocities and decreases for higher velocities.

### 4.3. Bubble rise velocity and visible bubble flow rate

The model results were analyzed to establish a relationship between the bubble diameter and rise velocity. The velocity of a rising bubble was calculated by tracking the motion of the individual bubble centers. However, the bubble rise velocity varied strongly due to coalescence, break-up, and bubbles interacting directly with the wall. Especially smaller bubbles showed deviating behavior due to the influence of the neighboring bubbles: a wake of a bubble has a larger effect on a trailing small bubble than on a trailing large bubble. Thus, all the data was categorized into different bubble size groups and the rise velocity of all the bubbles in an individual size group was averaged to obtain the averaged rise velocity. The average rise velocity as a function of the bubble diameter predicted by the KTGF and the CVM for a particle diameter of 500 μm and a superficial gas velocity of $2u_{mf}$ is compared with different correlations from the literature in Fig. 8.

The correlation given by Pyle and Harrison (1967) for a two-dimensional system is best suited to describe an isolated bubble in which the influence of the bed geometry was not accounted for. It predicts a very low rise velocity. On the other hand, the correlation proposed by Hilligardt and Werther (1986) for three-dimensional systems accounts for the influence of the bed diameter and predicts the highest rise velocity for the considered particle size. The correlation given by Lim et al. (1993), valid for two-dimensional

Table 4
Exponent A and B in equation (6) predicted by the CVM and the KTGF

| Exponent A | | | Exponent B | | |
|---|---|---|---|---|---|
| Height | CVM | KTGF | Velocity | CVM | KTGF |
| 0.15 m | 0.44 | 0.49 | $1.5u_{mf}$ | 0.8 | 0.76 |
| 0.25 m | 0.41 | 0.47 | $2.0u_{mf}$ | 0.56 | 0.65 |
| 0.35 m | 0.39 | 0.41 | $2.5u_{mf}$ | 0.63 | 0.53 |
| 0.45 m | 0.36 | 0.36 | — | — | — |
| Average | 0.4 | 0.43 | Average | 0.66 | 0.65 |

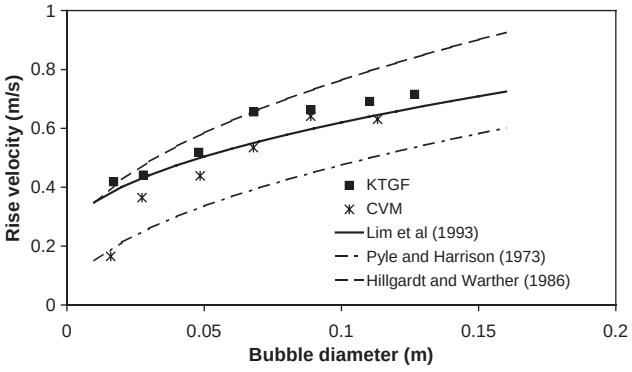


Fig. 8. Comparison of the average rise velocity as a function of the bubble diameter predicted by the KTGF and CVM with different correlations in the literature ($d_p = 500\,\mu\text{m}$, $u = 2u_{mf}$).

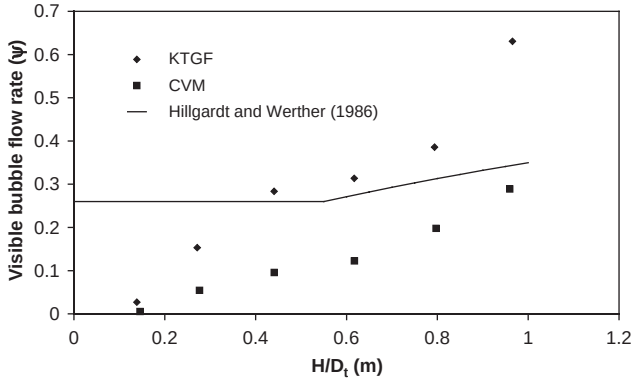


Fig. 9. Comparison of the visible bubble flow rate as a function of the relative height above the distributor predicted by KTGF and CVM and compared with the correlation proposed by Hilligardt and Werther (1986) ($d_p = 500\,\mu\text{m}$, $u = 2u_{mf}$).

systems, has been established for different ranges of particle sizes. The rise velocity predicted by the KTGF and the CVM was in the same order of magnitude for all these correlations and agrees particularly well with the correlation given by Lim et al. (1993). The KTGF model predicts a slightly higher rise velocity than the CVM for lower bubble sizes. However, for larger bubble sizes both the models predict the same bubble rise velocity. Although the KTGF model calculates the local shear viscosity in the bed, the average viscosity in the bed is in the same order of magnitude as the viscosity assumed in the CVM (1.0 Pa s), which results in approximately same resistance for the bubbles to rise through the bed. Therefore, the rise velocity of the bubble as a function of the bubble size is predicted the same by both models.

The classical two-phase model by Toomey and Johnstone (1952) assumes that the gas velocity in the emulsion phase equals the minimum fluidization and that all additional gas flows through the bed as visible bubbles. According to this model, the dimensionless visible bubble flow rate is expressed as

$$\psi = \frac{\dot{V}_b}{u - u_{mf}}. \tag{7}$$

However, the experimentally observed value of $\psi$ is always less than unity. The local visible bubble flow rate depends on the local bubble hold-up $\varepsilon_b$, and the local bubble rise velocity $u_b$. The average bubble holdup $\varepsilon_b$, was estimated by calculating the average bubble area in the individual bed section, divided by the area of the bed section. Thus, the dimensionless visible bubble flow can be expressed as

$$\Psi = \frac{\sum(A_b \cdot u_b)}{A_{\text{bed}}(u - u_{mf})}. \tag{8}$$

Fig. 9 shows a comparison of the dimensionless visible bubble flow rate predicted by the KTGF and the CVM for a particle diameter of 500 μm and a superficial gas velocity of $2u_{mf}$. The dimensionless visible bubble flow rate predicted by both models increases when the distance from the distributor increases. The fraction of visible bubble flow rate predicted by the KTGF agrees reasonably with the estimation given by Hilligardt and Werther (1986) (see Table 3). As shown before, by accounting for the dissipation of granular energy, larger bubbles were predicted by the KTGF model than the CVM, therefore the KTGF model predicts that less gas is percolating through the dense phase and more of the gas flow appears in the form of bubbles. Fig. 10 shows the measured visible bubble flow rate by Boemer et al. (1998)

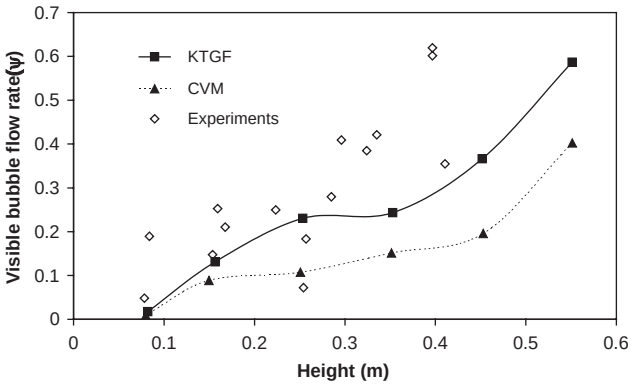


Fig. 10. Comparison of the visible bubble flow rate as a function of height above the distributor predicted by the KTGF and the CVM with experimental data obtained by Boemer et al. (1998) ($d_p = 692\,\mu m$, $u = 2u_{mf}$).

for a two-dimensional fluidized bed filled with 692 μm particles. Unlike the estimated values from the correlation by Hilligardt and Werther (1986), the experimental data shows a continuous increase in the visible bubble flow rate with increasing distance above the distributor, as also predicted by the two-fluid models. Again the predictions by the KTGF compare well with the experimental findings, while those by the CVM under-predict the visible bubble flow rate.

Concluding, at relatively low gas velocities the spontaneous bubble formation in a freely bubbling fluidized bed filled with Geldart B or D particles is dominated by the dissipation of granular energy due to particle–particle interactions, which is better described by the KTGF model. At higher gas velocities the bubble formation is mainly dominated by the non-linear drag, which explains the decreasing differences in the predictions by the KTGF and the CVM at higher gas velocities. The predicted average bubble size (number averaged) and visible bubble flow rate as a function of the distance above the distributor by the KTGF model is higher than that predicted by the CVM and agrees well with correlations from the literature and experimental measurements.

The KTGF model assumes instantaneous binary collisions and accounts for both kinetic and collisional contributions for the momentum and granular energy transfer in a particle ensemble. However, at high solids volume fractions, individual particles can interact under multiple neighbors with sustained contact, dominated by normal reaction forces and associated tangential frictional forces at these sliding contacts. These effects can be taken into account semi-empirically by adding frictional stresses in the momentum balance. The influence of the frictional stresses on the average bubble diameter, bubble rise velocity and visible bubble flow rate is studied next.

## 5. Influence of frictional stresses

Numerous attempts have been made in the past to describe the frictional stresses in a fluidized bed. A short overview of

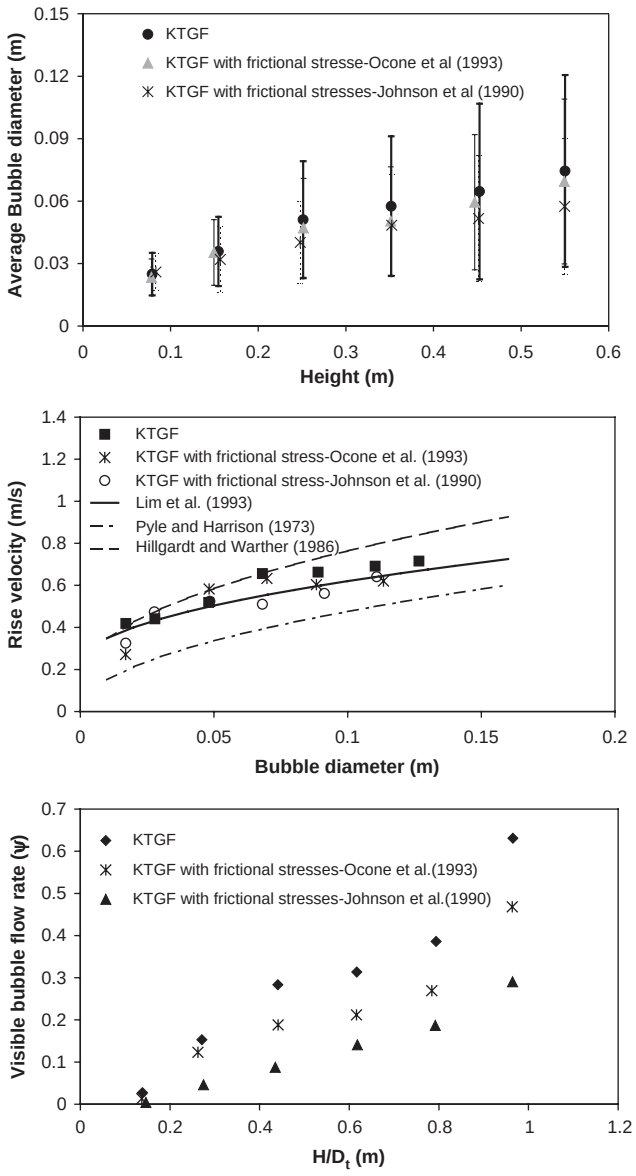


Fig. 11. Influence of the frictional stresses added in the KTGF model on the prediction of bubble size, rise velocity and visible bubble flow rate.

different approaches was presented in Part I. Fig. 11 shows the influence of the frictional stresses on the prediction of the number-averaged bubble diameter, rise velocity and visible bubble flow rate. With the addition of frictional normal stresses, the compaction of solids around the bubble interface is reduced, which increases the gas flow through the bubble boundary into the emulsion phase and therefore smaller bubbles are predicted. The prediction of the KTGF model varies significantly depending on the empirical constants used for the critical state pressure (see Table 5). Due to the higher critical state pressure predicted with the constants proposed by Johnson et al. (1990) even smaller bubbles were predicted when compared to model results using the constants proposed by Ocone et al. (1993).

Table 5
Values for the empirical parameters in the equation for the critical state pressure (Eq. (17) in Part I) (Johnson and Jackson, 1987) as suggested by different researchers

| $F$ (N/m$^2$) | $r$ | $s$ | $\varepsilon_{s,\min}$ | $\phi$ (deg) | $d_p$ (μm) | $\rho_s$(kg/m$^3$) | Material | Reference |
|---|---|---|---|---|---|---|---|---|
| 0.05 | 2 | 3 | 0.5 | 28 | 150 | 2500 | Unknown | Ocone et al. (1993) |
| 0.05 | 2 | 5 | 0.5 | 28.5 | 1000 | 2900 | Glass | Johnson et al. (1990) |

The predicted rise velocity of the bubble as a function of bubble size is marginally influenced by the frictional stresses. Due to the additional viscosity caused by the frictional stresses, the rise velocity of the bubble is slightly reduced. The comparison of the predicted results with the correlations available in the literature showed that the predicted rise velocity is well in the range of estimated values from the correlations and in good agreement with the correlation given for a two-dimensional system (Lim et al., 1993). The KTGF, which includes the frictional stresses, predicts a lower visible bubble flow rate. A lower bubble size and lower bubble velocity results in a lower visible bubble flow rate. This also entails that a higher gas flow rate is predicted in the dense phase when using the frictional viscosity. The predicted values are also significantly influenced by the empirical constants used for the critical state pressure. The predicted values using the empirical constants proposed by Johnson et al. (1990) are again much lower than the values predicted using the constants proposed by Ocone et al. (1993).

Concluding, the added frictional solid stresses have a significant influence on the bubble size, bubble rise velocity and visible bubble flow rate. The frictional stresses are very important in dense solid regions and the model predictions strongly depend on the empirical constants. Furthermore, the experiments to obtain the empirical constants of the frictional stresses are very difficult. Therefore, lower level modeling such as discrete particle modeling, should give more insight in the linking between particle–particle interactions and frictional stresses, in order to develop better closure equations accounting for frictional stresses based on a more fundamental footing.

## 6. Conclusions

In a freely bubbling fluidized bed at relatively low superficial gas velocities, bubble formation originates from inelastic particle–particle interactions. The KTGF model which accounts for the local dissipation of granular energy by particle collisions, predicts much larger bubbles with a much sharper interface compared to the CVM that predicts small and very diffuse bubbles. A quantitative comparison of the average bubble diameter predicted by both models showed that the bubble diameter predicted by KTGF was larger than that predicted by the CVM and agrees well with available correlations and experimental data published in the literature. However, the method of averaging of the simulated results requires careful consideration in the calculation of the mean bubble diameter. With an increase in the superficial gas velocity both models showed an increase in the bubble size. The rise velocity of the bubbles, especially of the larger bubbles, predicted by the KTGF and the CVM was approximately the same and consistent with correlations from the literature. The visible bubble flow rate predicted by the KTGF was much higher than that predicted by the CVM and matches well with experimental correlations and data.

The frictional solid stresses have a significant influence on the bubble size, bubble rise velocity and visible bubble flow rate. Accounting for the frictional stresses results in smaller bubbles due to increased leakage of gas through the bubble boundary and a lower bubble rise velocity and therefore the visible bubble flow rate is also reduced.

Although the KTGF model was in good agreement with the experimental data and correlations from the literature compared to the CVM for the prediction of bubble size distribution, bubble rise velocity and visible bubble flow rate, the model requires further development to incorporate the effect of the frictional stresses on a more fundamental basis. The current semi-empirical frictional stress models are inadequate since the model predictions strongly depend on empirical constants, which are difficult to determine experimentally.

## Notation

| | |
|---|---|
| $A_b$ | bubble area, m$^2$ |
| $A_0$ | catchment area, m$^2$ |
| $\boldsymbol{C}$ | fluctuating velocity of the particulate phase, m/s |
| $C_d$ | drag coefficient |
| $c$ | compaction modulus |
| $D_b$ | bubble diameter, m |
| $D_{ij}$ | strain rate, 1/s$^2$ |
| $D_0$ | diameter of the bubble at the distributor, m |
| $D_t$ | bed diameter, m |
| $d_p$ | particle diameter, μm |
| $e$ | restitution coefficient for particle–particle collision |
| $e_w$ | restitution coefficient for particle–wall collisions |
| $F$, $r$ and $s$ | empirical constants for the critical state pressure (Eq. (17) in Part I) |
| $G(\varepsilon_f)$ | elastic modulus, Pa |

| | |
|---|---|
| $G_0$ | elastic modulus at $\varepsilon_f = \varepsilon_f^*$, Pa |
| $g$ | gravity constant, m/s$^2$ |
| $g_0$ | solid radial distribution function |
| $h$ | height above distributor, m |
| $\boldsymbol{I}$ | unit vector |
| $m$ | mass of a particle, kg |
| $N$ | number of bubbles |
| $p$ | pressure, N/m$^2$ |
| $p_c$ | critical state pressure, N/m$^2$ |
| $q_s$ | kinetic fluctuation energy flux, kg/m s |
| $Re_p$ | particle Reynolds number |
| $u_{mf}$ | superficial gas velocity at minimum fluidization condition, m/s |
| $u_b$ | bubble rise velocity, m/s |
| $u$ | superficial gas velocity,m/s |
| $\bar{\boldsymbol{u}}$ | mean gas phase velocity, m/s |
| $\dot{V}_b$ | visible bubble flow rate, m/s |
| $\bar{\boldsymbol{v}}$ | mean solid phase velocity, m/s |

*Greek letters*

| | |
|---|---|
| $\alpha_s$ | specularity coefficient |
| $\beta$ | interphase drag coefficients, kg/m$^3$ s |
| $\gamma$ | dissipation rate, kg/m s$^3$ |
| $\varepsilon$ | volume fraction |
| $\varepsilon_b$ | bubble hold up |
| $\varepsilon_s^{\max}$ | solid volume fraction at packed condition ($=0.64356$) |
| $\Theta$ | granular temperature, m$^2$/s$^2$ |
| $\boldsymbol{\kappa}$ | conductivity of the granular fluctuating motion, kg/m s |
| $\lambda$ | bulk viscosity, kg/m s |
| $\mu$ | shear viscosity, kg/m s |
| $\boldsymbol{\tau}$ | shear stress tensor, Pa |
| $\rho$ | density, kg/m$^3$ |
| $\rho_{\mathrm{em}}$ | density of the emulsion phase, kg/m$^3$ |
| $\phi$ | angle of internal friction |
| $\phi_s$ | sphericity |
| $\psi$ | dimensionless visible bubble flow rate |

*Subscripts*

| | |
|---|---|
| $f$ | gas phase |
| $s$ | solid phase |
| $w$ | wall |

*Superscript*

| | |
|---|---|
| $kc$ | kinetic and collisional contribution |
| $f$ | frictional contribution |

## Appendix A. Grid dependency

Simulations were carried out with the CVM for a coarse grid (0.0075 m× 0.01 m) and fine grid (0.005 m × 0.005) to study the grid dependency of the solution. The difference in the time-averaged average bubble size calculated with these grids is within 5% (see Fig. 12).

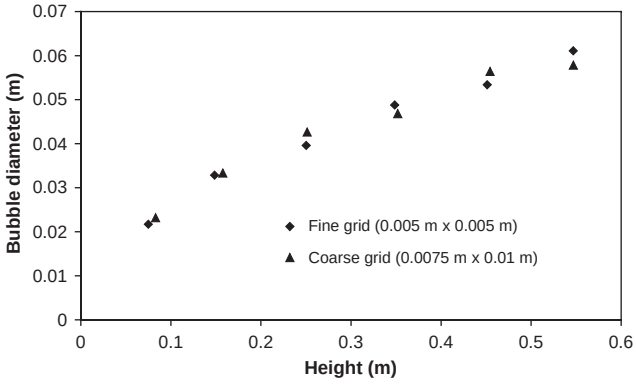


Fig. 12. Comparison of the number-averaged bubble diameter calculated for different grid sizes.

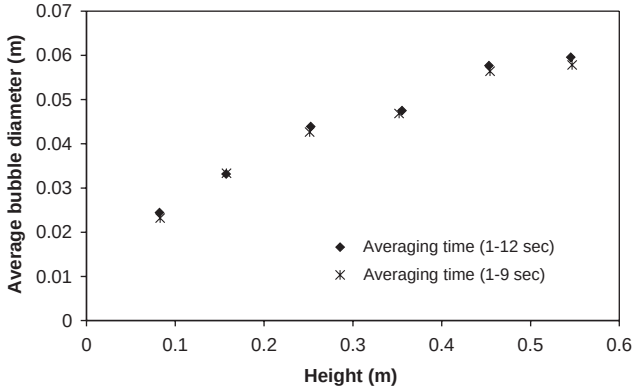


Fig. 13. Influence of the averaging time on the time-averaged results calculated using the CVM ($d_p = 500\,\mu$m, $u = 2u_{mf}$).

## Appendix B. Influence of the averaging time

Fig. 13 shows the influence of the averaging time on the predicted average bubble size calculated with the CVM. The calculated average bubble diameter is not influenced by the increasing averaging time compared to the time interval of 1–9 s.

## References

Boemer, A., Qi, H., Renz, U., 1998. Verification of Eulerian simulation of spontaneous bubble formation in a fluidized bed. Chemical Engineering Science 53, 1835–1846.

Darton, R.C., LaNauze, R.D., Davidson, J.F., Harrison, D., 1977. Bubble growth due to coalescence in fluidized beds. Transactions of the Institutions of Chemical Engineers 55, 274–280.

Davidson, J.F., Harrison, D., 1963. Fluidized Particle, Cambridge University Press, Cambridge.

Ding, J., Gidaspow, D., 1990. A bubbling fluidization model using theory of granular, flow. A.I.Ch.E. Journal 36, 523–538.

Geldart, D., 1973. Types of gas fluidization. Powder Technology 7, 285.
Gidaspow, D., Ettehadieh, B., 1983. Fluidization in two-dimensional beds with a jet. 2: hydrodynamic modeling. Industrial & Engineering Fundamentals 22, 193–201.
Hilligardt, K., Werther, J., 1986. Local bubble gas hold-up and expansion of gas/solid fluidized beds. German Chemical Engineering 9, 215–221.
Hoomans, B.P.B., Kuipers, J.A.M., Briels, W.J., van Swaaij W.P.M., 1996. Discrete particle simulation of bubble and slug formation in a two-dimensional gas-fluidised bed: A hard-sphere appraoch. Chemical Engineering Science 51, 99–108.
Johnson, P.C., Jackson, R., 1987. Frictional-collisional constitutive relations for granular materials, with application to plane shearing. Journal of Fluid Mechanics 176, 67–93.
Johnson, P.C., Nott, P., Jackson, R., 1990. Frictional-collisional equations of motion for particulate flows and their application to chutes. Journal of Fluid Mechanics 210, 501–535.
Kuipers, J.A.M., 1990. A two-fluid micro balance model of fluidized bed. Ph.D. Thesis, Twente University, Enschede, The Netherlands.
Lim, K.S., Gururajan, V.S., Agrawal, P.K., 1993. Mixing of homogeneous solid in bubbling fluidized beds: theoretical modeling and experimental investigation using digital image analysis. Chemical Engineering Science 48, 2251–2265.
Molerus, O., 1982. Interpretation of Geldart's type a,b,c,d powders. Powder Technology 33, 81–87.
Ocone, R., Sundaresan, S., Jackson, R., 1993. Gas–particle flow in a duct of arbitrary inclination with particle–particle interactions. A.I.Ch.E. Journal 39, 1261–1271.
Pyle, D.L., Harrison, D., 1967. The rising velocity of bubbles in two-dimensional fluidized beds. Chemical Engineering Science 22, 531.
Toomey, R.D., Johnstone, H.F., 1952. Gas fluidization of solid particles. Chemical Engineering Progress 48, 220–226.
van Wachem, B., 2000. Derivation, implementation, and validation of computer simulation models for gas-solid fluidized beds. Ph.D. Thesis. Delft University of Technology, The Netherlands.
Werther, J., 1974. Bubbles in gas fluidized beds—Part I. Transactions of the Institutions of Chemical Engineers 52, 149–159.
Werther, J., Molerus, O., 1973. The local structure of gas fluidized beds: I A statistically based measuring system. International Journal of Multiphase Flow 1, 103–122.